phys. stat. sol. (a), 1–10 (2003) / **DOI** 10.1002/pssa.200306675

Physical nature of grown-in microdefects in Czochralski-grown silicon and their transformation during various technological effects

V. I. Talanin* and **I. E. Talanin**

Zaporozhye State Engineering Academy, Lenin Avenue 226, 69006 Zaporozhye, Ukraine

Received 10 December 2002, revised 30 July 2003, accepted 1 August 2003
Published online 14 November 2003

PACS 61.72.Bb, 61.72.Ji, 61.72.Yx

Czochralski-grown dislocation-free silicon crystals of 50 and 80 mm in diameter have been extensively studied by techniques of transmission electron microscopy and preferential etching. Crystals were grown at various growth rates, followed by subsequent processing (thermal treatment, ion implantation). The physical nature (positive/negative sign of silicon lattice imperfection) of grown-in microdefects inside and within the OSF ring was determined. It was found that background oxygen and carbon impurities mostly affect the formation mechanism of grown-in microdefects. It was shown that crystals might grow in interstitial and interstitial–vacancy regimes. The transformation scheme of the grown-in microdefects in the course of subsequent processing is clarified.

1 Introduction

Czochralski-grown dislocation-free silicon crystal (CZ-Si) has a wide range of applications in modern semiconductor electronics. However, in the course of CZ-Si growth and subsequent cooling, structural imperfections, so-called "grown-in microdefects", occur. It is found that CZ-Si contains A, B and D microdefects, which differ from each other by etching pit dimensions and distribution shapes [1, 2]. In these two papers it was suggested that CZ-Si microdefects are similar to the grown microdefects that occur in float zone silicon (FZ-Si). From preferential etching images (uniform microdefect distribution) and X-ray topography images, the vacancy nature of D microdefects (negative sign of lattice imperfection) was assumed [3]. Coming from this, V. V. Voronkov developed a theoretical model of the formation mechanism of CZ-Si grown-in microdefects [4]. Recently, this model was applied to FZ-Si crystals [5, 6]. Voronkov's common model is based on the following: 1) there is a recombination between intrinsic point defects at temperatures close to the melting point; 2) there are independent areas with only interstitial-type (A and B microdefects) or vacancy-type microdefects (D microdefects); and 3) there is a critical parameter $C_{crit} = V/G$ (where V is the crystal growth rate, and G is the axial temperature gradient). When $V/G < C_{crit}$, self-interstitials dominate in the crystal (interstitial-type crystal growth), and when $V/G > C_{crit}$, vacancies dominate in the crystal (vacancy-type crystal growth).

In the past decade, grown-in microdefects have been revealed in large-diameter CZ-Si crystals and, depending on observation technique, were called FP defects (flow pattern defects), COP defects (crystal-originated particles), and LST defects (light-scattering tomography defects) [7, 8]. They all were identified as D microdefects [9]. With transmission electron microscopy (TEM) observation, their octahedral structure and sizes 100 to 300 mm were shown [10, 11]. As the oxygen concentration in the center of a defect is less than on its walls, they were suggested as "microvoids". This confirmed Voronkov's model

* Corresponding author: e-mail: V.I.Talanin@mail.ru, Fax: +38 0612 601498

in a certain manner. Furthermore, it has been reported that defects observed beyond the ring of OSF defects and below the ring of OSF defects constitute dislocation loops and interstitial-type clusters of point defects [12–15].

It should be noticed that these results contradict our experimental data of grown-in microdefects in FZ-Si crystals [16, 17]. From TEM observations the above papers showed that D microdefects have a positive sign of lattice imperfection (interstitial nature), while the area with vacancy-type defects contains at the same time interstitial-type ones. Further, the transformation mechanism of interstitial defects was clarified: D microdefects → B microdefects → A microdefects [17]. Apparently, CZ-Si, in contrast to FZ-Si, contains many more background impurities of oxygen and carbon, and different growth conditions prevail here. Still, from our viewpoint, the formation mechanisms of defects in CZ-Si and FZ-Si must be similar.

Therefore we conducted a thorough study (preferential etching, TEM) of CZ-Si single crystals to determine the sign of deformation for defects observed inside and within the ring of OSF defects.

2 Experimental methods

CZ-Si n-type crystals of 50 and 80 mm in diameter with ρ = 10–50 Ω cm were grown in argon medium in direction ⟨111⟩, oxygen concentration ~(4–7) × 10^{17} cm^{-3}, carbon concentration ~(5–7) × 10^{16} cm^{-3}. Oxygen and carbon concentrations were determined by infrared absorption spectra. The crystals were grown at constant growth rates ranging from 0.5 to 3 mm/min. Several crystals were grown at a special-purpose changing growth rate. To obtain implanted structures we used CZ-Si single crystals, 50 mm in diameter, grown at rates V = 0.5, 1.0 and 2.5 mm/min. Wafers, cut out of crystal parts where V = 0.5 mm/min (A and B microdefects) and V = 2.5 mm/min (uniform defect distribution), were implanted with arsenic (energy 65 keV, dosage ~3.7 × 10^{15} cm^{-2}). Other wafers, cut out of crystal parts where V = 1.0 mm/min, were implanted with antimony (energy 65 keV, dose ~3 × 10^{15} cm^{-2}). Afterwards the plates thus obtained were subjected to 5 hours annealing under 650 °C or 850 °C. Wafers not annealed were also studied.

We used a preferential etching technique to observe the distribution patterns of grown-in microdefects in (111) and (112) surfaces [18]. The samples for TEM were cut based on these patterns. The sample crystal surface was (111); sample diameter was 3 mm. The sample preparation procedure is described in [19]. The samples were observed by electron microscope under an accelerating voltage of 100 kV. Such conditions prevent radiation-induced defects [20]. The nature of the grown-in microdefects (sign of lattice imperfection) was determined by the black–white contrast method [21], 2.5D method [22] and inside–outside contrast method [23].

3 Results

3.1 Grown-in microdefects

Striated distribution of A and B microdefects was observed throughout the whole length of the CZ-Si 50 mm crystals grown at V = 0.5–2 mm/min (Fig. 1a). Figure 1b shows that at V = 2 mm/min the striated distribution in the center of the crystal disappears. Figure 2 depicts the uniform defect distribution in the center of the crystal and the striated defect distribution at the periphery at V = 2.5 mm/min.

When CZ-Si 50 mm crystals are grown at a changing growth rate, an area of uniform defect distribution (Fig. 2) is formed at V > 2 mm/min with its diameter increasing as the growth rate rises (Figs. 3 and 4). Quite often preferential etching does not reveal the defects in the center of the crystal. However, in this case, the central region is surrounded by a high-density uniform defect distribution (Figs. 3 and 4). According to classification [24] and research presented in [1, 2], we identified these defects as D microdefects that correspond to D microdefects in FZ-Si. In surface (111) one can observe a ring of D microdefects containing a so-called “defect-free” area inside (Fig. 3).

It will be observed that this ring of defects is often called the OSF ring in publications. But “oxidation-induced stacking faults” do not pertain to grown-in microdefects, because they occur after different

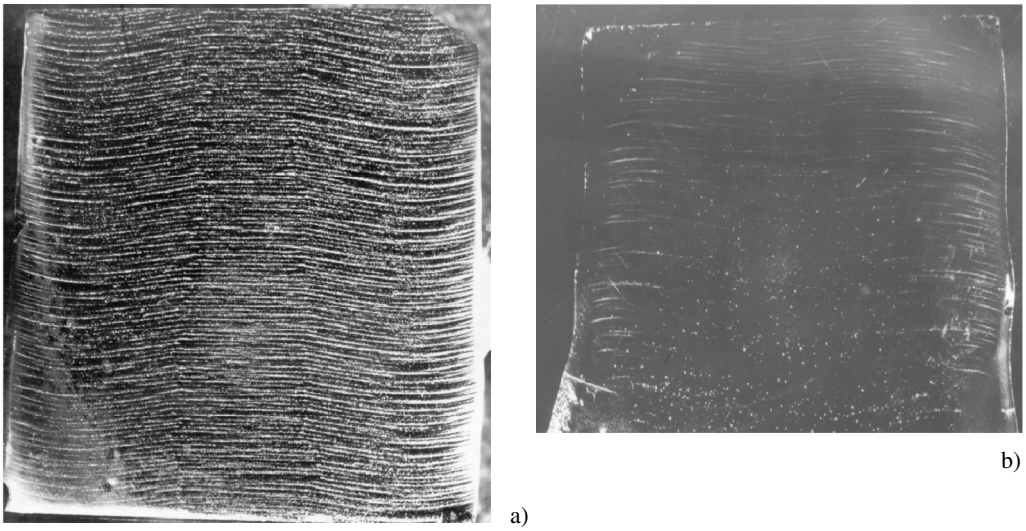

a) b)

Fig. 1 A and B microdefect distributions.

thermal treatment procedures [25, 26]. Recently it was reported that plate-like oxygen precipitates could be the source of their formation [27]. In our view this is an area of uniform distribution of grown-in D microdefects. As the growth rate increases, the ring of D microdefects moves to the crystal periphery while the "defect-free" area inside the ring increases in diameter. At V = 3 mm/min the ring of D microdefects disappears completely.

We conducted TEM directly within the ring of D microdefects and inside this ring (in the "defect-free" area). Within the ring of D microdefects we observed black–white contrast defects. Their concentration was 10^{13} to 10^{14} cm^{-3}, and their size was 4 to 12 nm. A. Bourret [28] was the first to observe these defects in CZ-Si; however, the sign of lattice imperfection has not been determined yet. By black–white and 2.5D methods we determined that these defects only induce interstitial-type CZ-Si lattice strain (Fig. 5). In the defect-free area inside the ring of D microdefects, we observed defects of the same size and concentration. The contrast analysis of TEM images showed both vacancy-type and interstitial-type defects. To establish the defect nature by the black–white contrast method we determined the sign of the product $\overline{g} \cdot \overline{\ell}$ on images obtained in dynamic conditions and also determined the defect depth to avoid ambiguities in the interpretation of the black–white contrast. We applied the stereomicrophotography of crystals to determine the defect depth. We investigated 500 specimens to establish the statistical relevance of our results. TEM observation of CZ-Si grown at V = 3 mm/min also proved the coexistence of

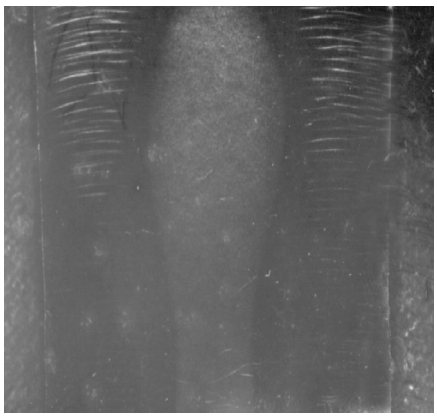

Fig. 2 Formation of area with uniform microdefect distribution in crystal grown at V = 2.5 mm/min in surface (112).

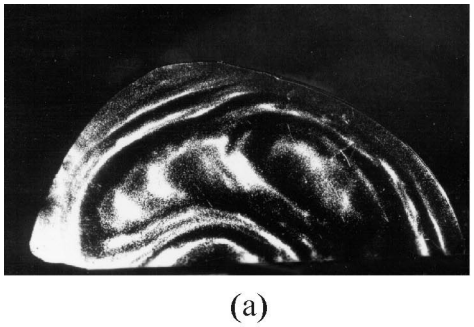

(a)

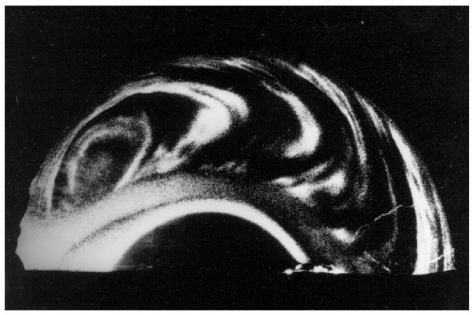

(b)

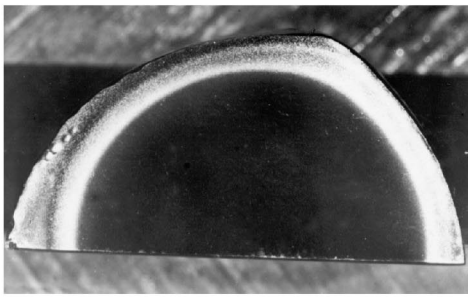

(c)

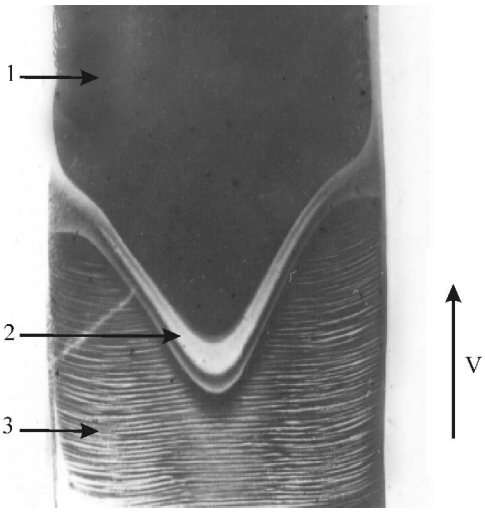

Fig. 3 Microdefect distribution in surface (111). A "defect-free" area is in the center and the ring of D microdefects is surrounding it.

both vacancy-type and interstitial-type microdefects (Fig. 6). The experimental results obtained are consistent with experimental results for FZ-Si [17]. As the strain field around the defect exceeds the defect size, the shape of the defect is not visible. Thus, for vacancy microdefects it cannot be exactly defined whether it is an "empty space" or oxygen–vacancy aggregate.

A background oxygen impurity is an important factor influencing the formation mechanism of the grown-in microdefects. And a carbon background impurity is as important as above, especially for FZ-Si [16, 17]. To clarify their particular effect on the formation mechanism of grown-in microdefects in CZ-Si, we studied the crystals grown at a growth rate changing from 1.8 to 0.8 mm/min. Crystals of 80 mm in diameter were obtained in direction ⟨111⟩ and were boron-doped to $\rho = 10$–$20\ \Omega$ cm. To reveal the defects of surface (111) we use a preferential etching technique. From the crystal micrographs one can observe areas of swirl microdefect distributions close to the periphery (Fig. 3b). There is a "defect-free" area in the central part of the crystal. Figure 7 depicts the micrographs of the crystal areas with different concentration of oxygen and carbon, where one can see different etch patterns for crystals with different concentrations of oxygen and carbon. The etching pits in the crystals with the same concentration of carbon, $\sim(4\text{–}5) \times 10^{16}$ cm^{-3} (Figs. 7a, b) have a round shape and a small depth. Etch patterns in the crystal with larger carbon content ($\sim 1.3 \times 10^{17}$ cm^{-3}) (Fig. 7c) are characterized by more distinct bordering and larger depth (from 1 to 1.5 μm). Table 1 summarizes the carbon and oxygen distributions in the crystal traverse section parallel to the

Fig. 4 Increasing of "defect-free" area in crystal grown at various growth rates, the site at V = 1.8–2.8 mm/min in surface (112): 1 – "defect-free" area with (I + V) microdefects; 2 – ring of D microdefects (OSF after thermal processing); 3 – A and B microdefects.

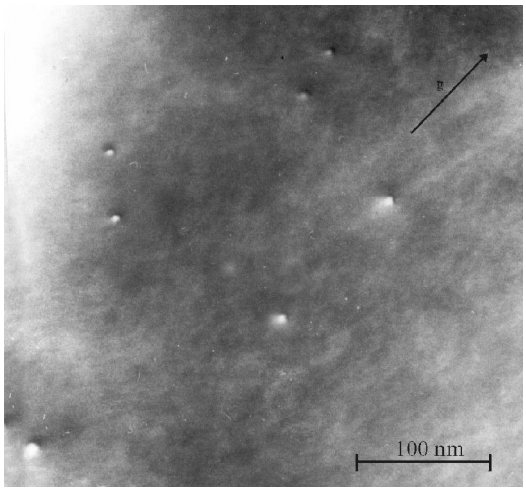

Fig. 5 The defects within the "ring", $\overline{g} = (\overline{2}20)$.

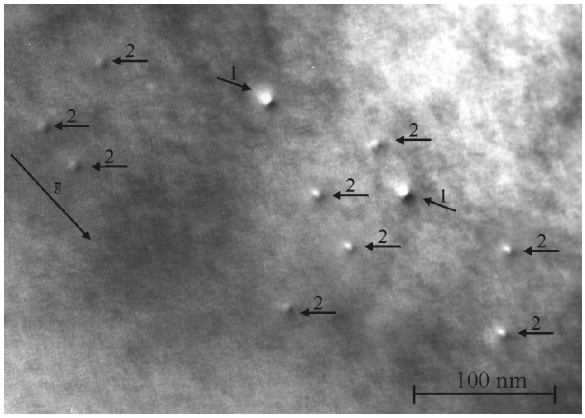

Fig. 6 Vacancy (1) and interstitial (2) microdefects inside the "ring", $\overline{g} = (\overline{2}02)$.

growth direction and the defect concentration measured at the same points. Evidently, the points with maximum carbon concentration and the points with maximum density of microdefects coincide.

However, if microdefect concentration is considered as a function of carbon concentration in different CZ-Si crystals, the relationship will be a bit different. Then, as the carbon content increases to 5×10^{16} cm^{-3}, the concentration of grown-in microdefects oscillates (Table 2). When carbon concentration exceeds 5×10^{16} cm^{-3}, the concentration of microdefects tends to increase as carbon concentration rises. Apparently, when carbon concentration is below 5×10^{16} cm^{-3}, oxygen impurities are more important in the formation of microdefects.

3.2 Microdefects in CZ-Si crystals after processing

Processing procedures lead to the transformation of the grown-in microdefects. As a result, secondary microdefects are formed. The transformation of the grown-in microdefects in the course of processing (e.g. thermal treatment or ion implantation) provides information about the relaxation process of the supersaturated solid solution of point defects.

Table 1 Change in density of microdefects and the change in concentration of oxygen and carbon along the crystal length.

crystal length (cm)	microdefect density (cm^{-2})	oxygen concentration (cm^{-3})	carbon concentration (cm^{-3})
0	5×10^3	6×10^{17}	1×10^{16}
10.0	7×10^3	5.5×10^{17}	2×10^{16}
20.0	9×10^3	5×10^{17}	3.5×10^{16}
30.0	2×10^4	4×10^{17}	6×10^{16}
40.0	4×10^3	3×10^{17}	5×10^{16}

Table 2 Change in density of microdefects (N_2) as a function of carbon concentration (N_1).

N_1 (cm^{-3})	8×10^{15}	1×10^{16}	2×10^{16}	3×10^{16}	4×10^{16}	5×10^{16}	9×10^{16}	1×10^{17}	2×10^{17}
N_2 (cm^{-2})	4×10^3	3×10^3	2×10^4	4×10^3	1×10^4	5×10^3	2×10^4	4×10^4	6×10^4

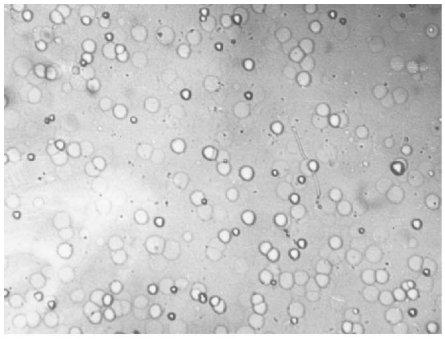

(a)

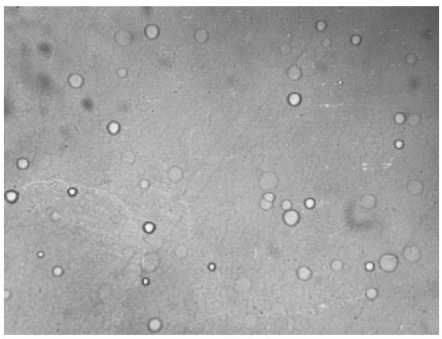

(b)

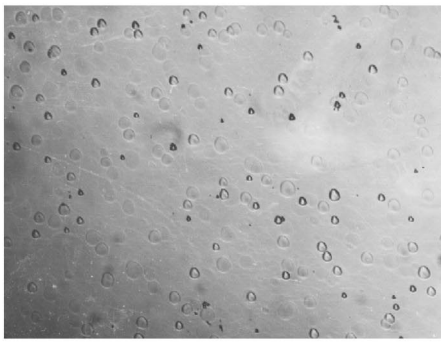

(c)

Fig. 7 CZ-Si crystal areas with different concentrations of background impurities (× 200, selective etching): a) oxygen is $(3.9–4.4) \times 10^{17}$ cm^{-3}, carbon is $(4.7–4.8) \times 10^{16}$ cm^{-3}; b) oxygen is $(3.6–3.8) \times 10^{17}$ cm^{-3}, carbon is $(4.2–4.6) \times 10^{16}$ cm^{-3}; c) oxygen is $(3.4–3.7) \times 10^{17}$ cm^{-3}, carbon is 1.3×10^{17} cm^{-3}.

A single crystal of CZ-Si, 50 mm in diameter, grown at V = 2.5 mm/min, was subjected to vacuum thermal treatment at 1100 °C for 10 hours. In the region of the OSF ring (in non-processed CZ-Si this was the ring of D microdefects), using TEM, we identified black–white contrast defects with sizes of 10 to 20 nm and defects having a strong strain contrast (precipitates) with sizes of 300 to 600 nm (Fig. 8). Inside the OSF ring complex-shaped defects are observed with sizes of 700 to 900 nm (Fig. 9).

Further, two phosphorus-doped CZ-Si crystals of 80 mm in diameter were grown at growth rates V = 0.6 mm/min (ρ = 18–30 Ω cm) and V = 2 mm/min (ρ = 7–10 Ω cm). The crystals were subjected to thermal treatment in the growing vessel at 650 °C for 1 hour in ambient air medium. We studied the distribution of microdefects in three areas located at the "top", "middle" and "bottom" of the crystals before and after thermal treatment. Table 3 summarizes the measurement results of defect density and carbon and oxygen concentrations. Carbon concentration increases towards the bottom part of the crystal. After thermal treatment the etching pit sizes become smaller and the swirl distribution in the bottom part of the crystal disappears. In CZ-Si crystals grown at V = 0.6 mm/min we identified big etching pits (~10^3 cm^{-2}) after thermal treatment, which were absent in crystals grown at V = 2 mm/min. Consequently, the view of microdefect distribution changes due to thermal treatment: the concentration of microdefects and their size increase steeply and the swirl distribution disappears in the bottom part of the crystal where carbon concentration is higher.

CZ-Si initial defect structure change due to ion implantation was the subject of a second series of experiments. CZ-Si crystal had grown-in microdefects of a certain type. CZ-Si crystal of 50 mm in diameter had a striated distribution of A and B microdefects in the region with a growth rate V = 0.5 mm/min, and a striated distribution of B microdefects in the region with a growth rate V = 1 mm/min. In the region with a growth rate V = 2.5 mm/min we used the area with both interstitial-type and vacancy-type microdefects.

It needs to be noted that the first two crystal growth regions indicate no substantial difference (crystals with A and B microdefects and crystals with B microdefects), so we will denote them as the crystal with (A + B) microdefects. Let us denote the crystal growth region with V = 2.5 mm/min as the crystal with (I + V) microdefects. We may compile experimental results obtained by TEM observation into three groups. The first group of results covers samples not subjected to annealing after ion implantation (I); the

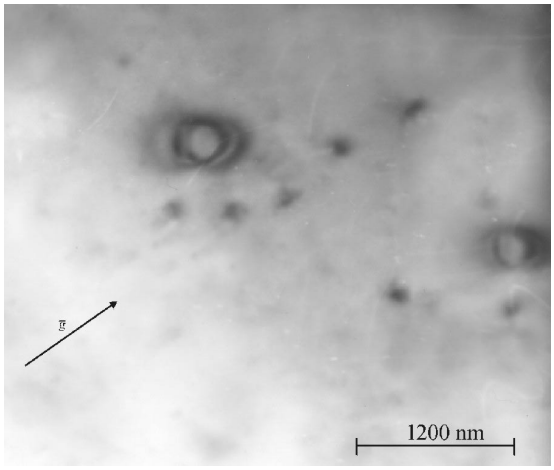

Fig. 8 Defects after thermal treatment in the "ring", $\bar{g} = (2\bar{2}0)$.

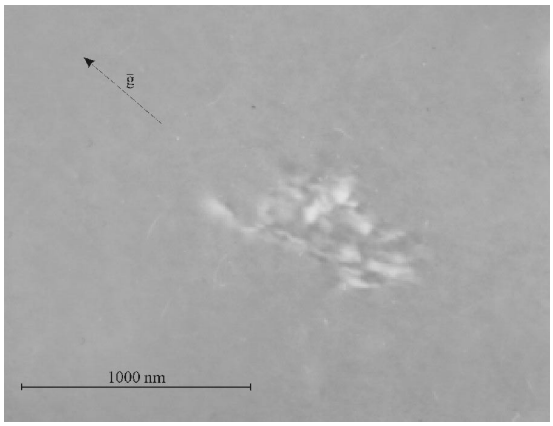

Fig. 9 Defects after thermal treatment inside the "ring", $\bar{g} = (2\bar{2}0)$.

second group covers samples subjected to annealing at 650 °C (II); and the third group covers samples subjected to annealing at 850 °C (III).

The study of group (I) samples with (A + B) microdefects revealed the following (Fig. 10):

a) small-scale defects with sizes ranging from 6 to 20 nm at concentration of $5 \times (10^8–10^9)$ cm^{-3};

b) precipitates of regular (square-shaped, rhomb-shaped) and irregular shape with sizes ranging from 30 to 100 nm;

c) dislocation loops with sizes ranging from 30 to 150 nm.

The concentration of precipitates amounted to $3 \times (10^8–10^9)$ cm^{-3} and the concentration of dislocation loops was $4 \times (10^8–10^9)$ cm^{-3}. Imperfections of the similar type were found in samples with (I + V) microdefects, but their sizes were two or three times smaller. At the same time, the concentration of precipitates and concentration of dislocation loops were one order of magnitude smaller than those in the samples with (A + B) microdefects.

The study of group (II) samples with (A + B) microdefects revealed the following (Figs. 11 and 12):

a) small-scale defects with sizes ranging from 4 to 20 nm;

b) precipitates with sizes ranging from 30 to 100 nm;

c) dislocation loops with sizes of 20 to 40 nm;

d) straight dislocation segments being angled to surface (111);

e) hexagonal formations with dimensions 160 × 80 nm to 600 × 240 nm.

Table 3 Density of microdefects and concentration of background impurities in crystals before and after thermal treatment (T = 650 °C, t = 1 h).

growth rate (mm/min)	oxygen concentration (cm^{-3})		carbon concentration (cm^{-3})		microdefect density in plane (111) (cm^{-2})			
					before treatment		after treatment	
	center	rim	center	rim	center	rim	center	rim
2.0 ("top")	3.7×10^{17}	3.2×10^{17}	4.8×10^{16}	5×10^{16}	2.3×10^4	2.8×10^4	3.9×10^4	4.9×10^4
2.0 ("middle")	3.4×10^{17}	3×10^{17}	7.9×10^{16}	7.6×10^{16}	2.8×10^4	2.7×10^4	4×10^4	3.2×10^4
2.0 ("bottom")	3×10^{17}	2.8×10^{17}	1.5×10^{17}	1.6×10^{17}	2.3×10^4	2.9×10^4	2.5×10^5	4×10^4
0.6 ("top")	3.8×10^{17}	1.9×10^{17}	4.6×10^{16}	4.5×10^{16}	2.6×10^4	1.9×10^4	4.5×10^4	1.1×10^5
0.6 ("middle")	3.5×10^{17}	2.9×10^{17}	5.9×10^{16}	5.3×10^{16}	1.8×10^4	2.8×10^4	4.4×10^4	5×10^4
0.6 ("bottom")	3.7×10^{17}	1.8×10^{17}	8.6×10^{16}	8.9×10^{16}	2.6×10^4	2.8×10^4	3×10^5	9.6×10^4

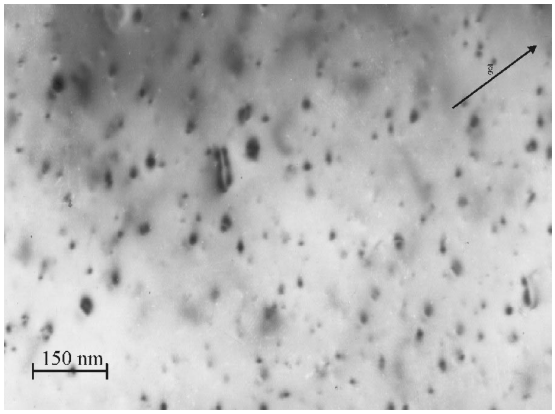

Fig. 10 The defects after arsenic implantation without annealing, dark field, $\overline{g} = (\overline{2}20)$.

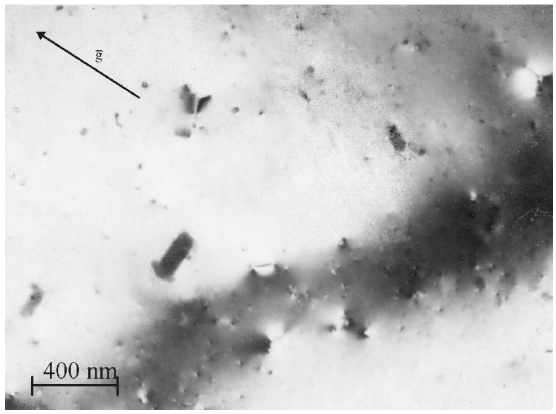

Fig. 11 The defects after arsenic implantation and annealing at 650 °C, dark field, $\overline{g} = (2\overline{2}0)$.

Group (II) samples contain a higher concentration of small-scale defects, precipitates and dislocation loops by one to two orders of magnitude as compared to those of group (I). The concentrations of dislocations and hexagonal formations are ~10^7 cm^{-3}. Apparently, these formations represent hexagonal stacking faults [29]. In group (II) samples with (I + V) microdefects, the concentrations of all the imperfections observed were smaller by one to two orders of magnitude, while straight dislocation segments were not found.

The study of group (III) samples with (A + B) microdefects revealed the following (Fig. 13):

a) small-scale defects with sizes ranging from 4 to 20 nm;

b) precipitates with sizes ranging from 30 to 130 nm;

c) dislocation loops with sizes ranging from 40 to 100 nm;

d) straight dislocation segments;

e) hexagonal formations.

The concentration of small-scale defects, precipitates and dislocation loops in samples of group (III) decreases by one to two orders of magnitude as compared to samples of group (II). Precipitates often occur as plate-like formations in the shape of square, rhombus or rectangle. In samples of group (III) with (I + V) microdefects, the concentrations of all the imperfections observed were one to two orders of magnitude smaller, while straight dislocation segments were not found.

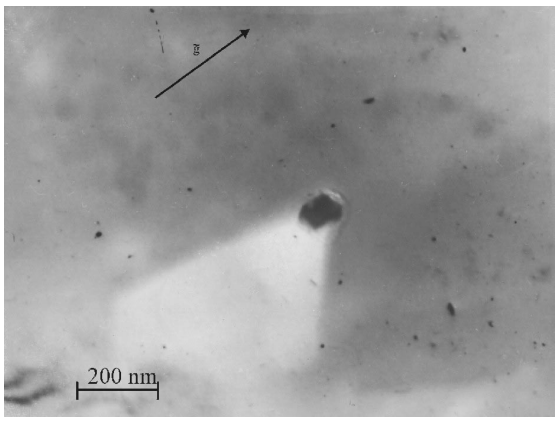

Fig. 12 The defects after antimony implantation and annealind at 650 °C, dark field, $\overline{g} = (\overline{2}20)$.

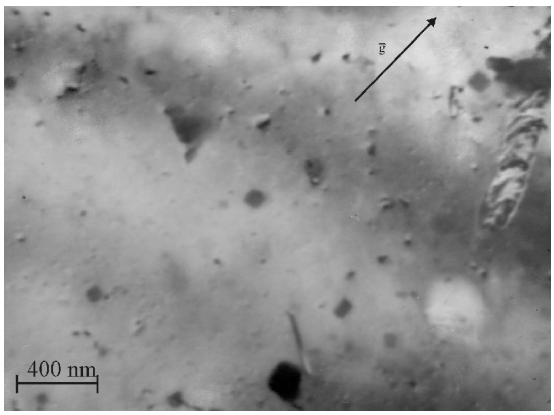

Fig. 13 The defects after arsenic implantation and annealing at 850 °C, dark field, $\overline{g} = (\overline{2}20)$.

Analysis of the obtained experimental results shows that in the course of ion implantation and further technological annealing, CZ-Si grown-in microdefect growth and transformation occur, following by relaxation of the supersaturated solid solution of point defects. The transformation of the structural imperfections is as follows: grown-in microdefects + point defects → dislocation loops + precipitates → plate-like formations + dislocations.

4 Discussion

Experimental results obtained within the framework of the study of the sign of defect-induced lattice imperfection (defect physical nature) in small-diameter CZ-Si crystals are of significant importance. They show that defects located within the ring of D microdefects are of interstitial type, while inside the ring of D microdefects one can observe both vacancy-type and interstitial-type microdefects. This means that there is no pure vacancy-type CZ-Si crystal growth, but rather interstitial-type and vacancy–interstitial-type growth. In this case the parameter $V/G = C_{crit}$ determines the conditions when vacancy-type microdefects, along with interstitial-type ones, occur or vanish. The circumstance that both types of microdefects coexist means that recombination of intrinsic point defects close to the crystal–melt interface is greatly hindered because of an energy barrier.

These experimental results contradict Voronkov's common theoretical model [4, 5], although they are consistent with Hu's [30] theoretical assumption that intrinsic point defects occur independently at high temperatures. So, the formation mechanism of the grown-in microdefects in CZ-Si will allow two independent directions in which the supersaturated solid solution of the point defects is relaxed. In [16, 17] we describe in detail the similar mechanism for FZ-Si crystals. The study of the nature of the grown-in microdefects in CZ-Si proves that the processes responsible for their formation are similar to those in FZ-Si. The differences arise from a greater concentration of oxygen and carbon background impurities and also from CZ-Si growth conditions in comparison with FZ-Si growth conditions.

Processing (ion implantation, thermal treatment) leads to the generation of a supersaturated solid solution of point defects. The initial grown-in microdefects facilitate the subsequent decomposing of this solution. This process leads to the transformation of the initial microdefects and the appearance of new imperfections. Low-temperature annealing of implanted CZ-Si at 650 °C induces dislocations and hexagonal stacking faults. However, such defects have not been found in implanted CZ-Si not subjected to thermal treatment. Apparently, low-temperature annealing entails a process in which some impurity atoms transit from lattice sites into interstitial ones [31]. The decrease in the defect concentration during annealing at 850 °C may be explained both by the decomposition of the oversaturated "silicon impurity" solid solution and by the diffusion process of the intrinsic point defects. The prismatic punch out mechanism induces the formation of dislocation loops, while their growth is connected with self-interstitials emitted by the growing precipitates.

Ion implantation to CZ-Si obtained by vacancy–interstitial-type growth indicates the general direction of the defect formation mechanism. The supersaturated solid solution of point defects forms in the course of implantation and consists of arsenic atoms, native point defects and background impurity atoms of carbon and oxygen. Other researchers [32] have pointed out that in such a case SiAs complex generation is more energy favorable, while VAs_2 complex generation is not proved experimentally [31]. SiAs complex generation is accompanied by the process in which free vacancies are absorbed by the interstitial-type microdefects. Thus, both interstitial-type microdefects grow emitting self-interstitial atoms of silicon that results in their excess number. Self-interstitials interact with the vacancy-type microdefects, which during transformation change their sign of imperfection from vacancy type to interstitial type.

Experimental results prove that the grown-in microdefect transformation due to processing is as follows: grown-in microdefects + point defects → dislocation loops + precipitates → plate-like formations + dislocations.

5 Conclusion

Depending on special conditions, especially on the *V*/*G* parameter, CZ-Si crystal may grow as either interstitial type or vacancy–interstitial type. The supersaturated solid solution of point defects is relaxed through two channels during the process of crystal cooling. Apparently, this is due to the existence of a recombination barrier for the point defects in CZ-Si. Background impurities of oxygen and carbon stimulate the formation mechanism of defects, being the formation centers of the grown-in microdefects.

References

[1] A. J. R. de Kock, W. T. Stacy, and W. M. van de Wijgert, Appl. Phys. Lett. **34**, 611 (1979).
[2] A. J. R. de Kock and W. M. van de Wijgert, J. Cryst. Growth **49**, 718 (1980).
[3] P. J. Roksnoer and M. M. B. van den Boom, J. Cryst. Growth **53**, 563 (1981).
[4] V. V. Voronkov, J. Cryst. Growth **59**, 625 (1982).
[5] V. V. Voronkov and R. Falster, J. Cryst. Growth **194**, 76 (1998).
[6] V. V. Voronkov and R. Falster, J. Cryst. Growth **198**, 399 (1999).
[7] K. Harada, H. Tanaka, T. Watanabe, and H. Furuya, Jpn. J. Appl. Phys. **37**, 3194 (1998).
[8] W. P. Lee, W. S. Seow, H. K. Yow, and T. Y. Tou, Jpn. J. Appl. Phys. **40**, 18 (2001).
[9] S. Umeno, Y. Yanase, M. Hourai, and M. Sano, Jpn. J. Appl. Phys. **38**, 5725 (1999).
[10] M. Kato, T. Yoshida, Y. Ikeda, and Y. Kitagawara, Jpn. J. Appl. Phys. **35**, 5597 (1996).
[11] M. Nishimura, S. Yoshino, H. Motoura et al., J. Electrochem. Soc. **143**, L243 (1996).
[12] S. Sadamitsu, S. Umeno, Y. Koike et al., Jpn. J. Appl. Phys. **32**, 3675 (1993).
[13] S. Iida, Y. Aoki, Y. Sugita et al., Jpn. J. Appl. Phys. **39**, 6130 (2000).
[14] N. Nango, S. Iida, and T. Ogawa, J. Appl. Phys. **86**, 6000 (1999).
[15] J. Furukawa, H. Tanaka, Y. Nakada, N. Ono, and H. Shiraki, J. Cryst. Growth **210**, 26 (2000).
[16] V. I. Talanin, I. E. Talanin, and D. I. Levinson, Semicond. Sci. Technol. **17**, 104 (2002).
[17] V. I. Talanin, I. E. Talanin, and D. I. Levinson, Cryst. Res. Technol. **37**, 983 (2002).
[18] E. Sirtl and A. Adler, Z. Met.kd. **52**, 529 (1961).
[19] C. J. Buiocchi, J. Appl. Phys. **38**, 1980 (1967).
[20] M. Pasemann and P. Werner, phys. stat. sol. (a) **54**, 179 (1979).
[21] M. F. Ashby and L. M. Brown, Phil. Mag. **8**, 1649 (1963).
[22] J. B. Mitchell and W. L. Bell, Acta Metall. **24**, 147 (1976).
[23] H. Föll and M. Wilkens, phys. stat. sol. (a) **31**, 519 (1975).
[24] N. V. Veselovskaya, E. G. Sheikhet, and E. S. Falkevich, in: Rost i Legirovanie Polyprovodnykovych Kristallov i Plenok, Vol. 2 (Nauka, Novosibirsk, 1977), p. 279 (in Russian).
[25] H. Shimizu, C. Munakata, N. Honma et al., Jpn. J. Appl. Phys. **31**, 1817 (1992).
[26] M. S. Bawa, W. L. Bell, H. M. Crimes, and T. J. Shaffner, J. Cryst. Growth **94**, 803 (1989).
[27] K. Harada, H. Furuya, and M. Kida, Jpn. J. Appl. Phys. **36**, 3366 (1997).
[28] A. Bourret, J. Thibault-Desseaux, and D. N. Seidman, J. Appl. Phys. **55**, 825 (1984).
[29] K. V. Ravi and C. J. Varker, J. Appl. Phys. **45**, 272 (1974).
[30] S. M. Hu, J. Vac. Sci. Technol. **14**, 17 (1977).
[31] V. P. Popov, A. V. Dvurechenskii, B. P. Kashnikov, and A. I. Popov, phys. stat. sol. (a) **94**, 569 (1986).
[32] A. Terrasi, E. Rimini, V. Raineri et al., Appl. Phys. Lett. **73**, 2633 (1998).